

ORIGINAL ARTICLE

Anti-tumor activity of obinutuzumab and rituximab in a follicular lymphoma 3D model

E Decaup^{1,2,3,4,5,6}, C Jean⁷, C Laurent^{8,9}, P Gravelle^{1,2,3,4,5}, S Fruchon⁸, F Capilla¹⁰, A Marrot¹⁰, T Al Saati¹⁰, F-X Frenois⁹, G Laurent^{1,2,3,4,5,11}, C Klein¹², N Varoquaux¹³, A Savina¹⁴, J-J Fournié^{1,2,3,4,5} and C Bezombes^{1,2,3,4,5}

Follicular lymphomas (FLs) account for 35–40% of all adult lymphomas. Treatment typically involves chemotherapy combined with the anti-CD20 monoclonal antibody (MAb) rituximab (RTX). The development of the type II anti-CD20 MAb obinutuzumab (GA101) aims to further improve treatment. Here, using FL cells we show that RTX and GA101 display a similar activity on RL cells cultured in 2D. However, 2D culture cannot mimic tumor spatial organization and conventional 2D models may not reflect the effects of antibodies as they occur *in vivo*. Thus, we created a non-Hodgkin's lymphoma (NHL) 3D culture system, termed multicellular aggregates of lymphoma cells (MALC), and used it to compare RTX and GA101 activity. Our results show that both antibodies display greater activity towards FL cells in 3D culture compared with 2D culture. Moreover, we observed that in the 3D model GA101 was more effective than RTX both in inhibiting MALC growth through induction of (lysosomal) cell death and senescence and in inhibiting intracellular signaling pathways, such as mammalian target of rapamycin, Akt, PLCgamma (Phospholipase C gamma) and Syk. Altogether, our study demonstrates that spatial organization strongly influences the response to antibody treatment, supporting the use of 3D models for the testing of therapeutic agents in NHL.

Blood Cancer Journal (2013) 3, e131; doi:10.1038/bcj.2013.32; published online 9 August 2013

Keywords: spatial organization; monoclonal antibodies; follicular lymphoma; 3D model

INTRODUCTION

Follicular lymphoma (FL) is the second most common type of B non-Hodgkin's lymphomas (NHL) and makes up 40% of all adult lymphomas. Although the prognosis of FL is variable, most patients with aggressive forms of FL (with a high FLIPI (Follicular Lymphoma International Prognostic Index) score) ultimately die from their disease and median survival is 5–8 years.¹ In recent years, impressive progress has been made in the treatment of NHL, mainly due to combining chemotherapy with rituximab (RTX), a monoclonal antibody (MAb) directed against the membrane-associated CD20 antigen.

Considerable efforts to characterize the mechanisms underlying the de-regulation of B-cell functions in NHL have identified the involvement of B-cell receptor components, various kinases such as Btk, Syk and PKC, as well as canonical pathways, including PI3K (phosphoinositide-3 kinase)/Akt or nuclear factor-kappaB modules.^{2–6} Signaling induced by RTX treatment involves raft microdomains and causes activation or inhibition of several pathways responsible for apoptosis or proliferation/survival (for reviews, see Bonavida² and Bezombes *et al.*³). Moreover, the efficacy of RTX is believed to involve antibody-mediated mechanisms of action such as complement-dependent cytotoxicity and antibody-dependent cell cytotoxicity through Fcγ receptor-expressing cells, such as NK cells, γδ T lymphocytes and macrophages.^{7,8} Although significant advances have been

achieved using RTX in both progression-free and overall survival, a significant number of cases remain incurable and patients develop RTX-refractory disease. Thus, novel anti-CD20 antibodies have been developed such as obinutuzumab (GA101), a glycoengineered type II CD20 antibody that induces enhanced antibody-dependent cell cytotoxicity and direct cell death compared with RTX. Unlike type I antibodies, type II antibodies do not translocate CD20 into raft microdomains and display less complement-dependent cytotoxicity than type I antibodies.^{9–11} GA101 also induces a non-apoptotic cell death involving homotypic adhesion, lysosomal permeabilization, cathepsin release and production of radical oxygen species (ROS).^{12,13} Phase I/II trials of GA101 have shown promising activity, and it is currently being studied in several pivotal trials in indolent NHL, diffuse large B-cell lymphoma and B-cell chronic lymphocytic leukemia.^{14,15}

Like most carcinomas, NHL grow as spherical tumors. Based on carcinoma 3D models (often described as spheroids), it is acknowledged that spatial organization may profoundly affect tumor cell behavior as important functions are dictated by the collective properties of a cell population rather than those of a single cell. These include growth, metastasis, cell-to-matrix and cell-to-cell interaction, as well as intracellular signaling and resistance to anti-tumor agents or even immune escape.^{16–19} Spatial organization can exert these effects in cancer cells by

¹INSERM UMR1037–Centre de Recherche en Cancérologie de Toulouse, Toulouse, France; ²Université Toulouse III Paul-Sabatier, Toulouse, France; ³ERL 5294 CNRS, BP3028, Hôpital Purpan, Toulouse, France; ⁴Institut Carnot Lymphome–CALYM, Toulouse, France; ⁵Laboratoire d'Excellence Toulouse Cancer–TOUCAN, Toulouse, France; ⁶Institut de Recherche Roche, Boulogne Billancourt, France; ⁷Moore's UCSD Cancer Center, Department of Reproductive Medicine, La Jolla, USA; ⁸INSERM UMR1043–Centre de Physiopathologie Toulouse Purpan, Toulouse, France; ⁹Service Anatomie Pathologique CHU Toulouse, Hôpital Purpan, Toulouse, France; ¹⁰INSERM, US006, ANEXPLO/CREFRE, Service d'Histopathologie, CHU Purpan, Toulouse, France; ¹¹Service d'Hématologie, CHU Purpan, Toulouse, France; ¹²Roche Glycart AG, Pharma Research and Early Development (pRED), Schlieren, Switzerland; ¹³F. Hoffmann-La Roche AG, Basel, Switzerland and ¹⁴Roche S.A.S, Boulogne Billancourt, France. Correspondence: Dr C Bezombes, Cancer Research Center of Toulouse, INSERM U1037, CHU Purpan, Toulouse 31024, France.

E-mail: christine.bezombes-cagnac@inserm.fr

Received 28 February 2013; revised 3 July 2013; accepted 15 July 2013

affecting gene expression profiles^{18,19} or influencing major signaling pathways, such as those driven by mitogen-activated protein kinase, Akt and oncogenic products, such as HER-2.²⁰ More importantly, spatial organization is known to influence the response to antibodies, such as Trastuzumab or Pertuzumab.^{20,21}

Conventional 2D NHL cell culture models do not reflect the true effects of antibodies as they occur *in vivo* and may be of limited use. Thus, we recently created a NHL 3D culture system, the so-called multicellular aggregates of lymphoma cells (MALC) model, using a modification of the 'hanging drop' method.²² This model is useful for evaluating tumor sensitivity to antibodies as diffusion/distribution is different within a solid 3D tumor.²³

Here, we sought to examine and compare the effects of GA101 and RTX in our 3D MALC model to gain a better understanding of the differences between these antibodies and to assess our model as a tool for effective *in vitro* studies into MAb efficacy.

MATERIALS AND METHODS

Cell lines and MABs

RL were obtained from the American Type Culture Collection (ATCC), Rockville, MD, USA, Raji from the ATCC and DEAU were kindly provided by Pr Delsol (CRCT, INSERM U1037, Toulouse, France). These cell lines were cultured at 37 °C in humidified 5% CO₂ atmosphere in a complete RPMI medium.

MALC preparation

MALC were obtained by the hanging drop method.²² Briefly, drops (20 µl) of 10⁴ RL, DEAU or Raji cells (day 0) in complete medium enriched with 1% methylcellulose (MethoCult H4230, StemCell Technologie, Grenoble, France) were placed onto the lid of a 24-well plate, which was then inverted over a plate containing 1 ml of medium. Hanging drop cultures were incubated for 24 h at 37 °C in 5% CO₂. In parallel, a layer of 1% agarose (Life Technologies, St Aubin, France) in classical medium was added to another 24-well plate and stored for 24 h at 4 °C. After 24 h, the resulting cellular aggregates were transferred to the agarose plate and cultured at 37 °C in 5% CO₂. MABs were applied to the initial drop and every 5 days thereafter.

MALC volume was calculated using the formula $V = 4/3 \times \Pi \times L \times l^2$ (where L is the longest diameter and l is the shortest diameter).

Morphology was visualized after Hoechst33342 (Invitrogen, Life Technologies) staining. MALC were incubated with Hoechst33342 (10 µg/ml) for 10 min at 37 °C in a CO₂ incubator.

Pictures were taken with a fluorescent inverted microscope Nikon Eclipse TE200 (Nikon, Champigny Sur Marne, France) at magnification $\times 40$.

Viable cell number was determined by counting cells on a Malassez hemocytometer (D. Dutscher, Brumath, France) using the trypan blue exclusion method.

RL lymphoma xenograft

A total of 10×10^6 RL cells were subcutaneously injected into the right flank of SCID-Beige mice, according to the INSERM Animal Care and Use Committee-approved protocol. When tumor volumes (TVs) reached 100 mm³, the mice were divided into three groups of 8–10 animals. Phosphate-buffered saline (PBS)-, RTX- or GA101-treated groups were injected intraperitoneally twice a week with 25 mg/kg MAB. Tumor burden was measured three times per week with a caliper, and TV calculated using the formula $(TV = (\text{length} \times \text{width}^2)/2)$. Animals were killed when the TV reached 2000–2500 mm³; tumor weight was measured at this time point. Tumors were embedded in paraffin and processed for immunohistochemistry labeling as described below.

Immunohistochemistry labeling

Immunostaining was performed using an automated stainer (Benchmark XT; Ventana Medical Systems, Tucson, AZ, USA). Antibodies directed against active anti-caspase 3 (R&D Systems, Lille, France), Ki67 (Abcam, Cambridge, UK), laminin and fibronectin (Sigma-Aldrich, Lyon, France) were used. After overnight incubation, sections were incubated with the avidin-biotin-peroxidase complex (Vectastain ABC kit, Clinisciences, Nanterre, France) followed by the 3,3'-diaminobenzidine chromogen

solution and were then counterstained with hematoxylin. Negative controls were incubated in buffered solution without primary antibody.

Caspase 3 active detection by confocal microscopy

Untreated or anti-CD20 MAB-treated MALC were fixed after 20 days in 4% paraformaldehyde. MALC were pretreated with 0.1 M sodium citrate pH 6.0 by microwave incubation, permeabilized with 0.1% saponin and stained overnight at 4 °C with anti-active caspase 3 antibody (a-CASP3; rabbit polyclonal, dilution 1:1000, Abcam) in PBS, 3% bovine serum albumin/4-(2-hydroxyethyl)-1-piperazineethanesulfonic acid and 0.1% saponin. Primary Ab was revealed by a goat anti-rabbit Ab labeled with Alexa 633 (Life Technologies) for 2 h at room temperature. Control was realized using the secondary Ab without anti-CASP3 Ab. Samples were mounted in Fluorescence Mounting Medium (DAKO, Les Ulis, France) and examined using a Zeiss LSM 710 confocal microscope (Carl Zeiss, Marly Le Roi, France) with a $\times 63$ Plan-Apochromat objective (1.4 oil). To detect Alexa 633 fluorescence, a helium laser was filtered at 633 nm. For each analyses, standardized conditions for pinhole size, gain and offset (brightness and contrast) were used for image capture.

In vivo caspase 3-positive cell quantification

Immunohistochemical-stained slides were digitized using a Panoramic 250 Flash digital microscope (P250 Flash, 3DHiTech, Budapest, Hungary). Whole slides were scanned using brightfield scan mode with a 20X/NA0.80 Zeiss Plan-Apochromat dry objective, and images were acquired with a two megapixel 3CCD color camera (CIS Cam Ref#VCC-F52U25CL, CIS Americas Inc., Tokyo, Japan), achieving a 0.22 µm/pixel resolution, corresponding to a $\times 56.09$ magnification at the highest optical resolution in conventional microscopy. Panoramic Viewer and HistoQuant software were used for viewing and analyzing the digital slides, respectively (RTM 1.15.0.53, 3DHiTech). A minimum of 12 annotations per slide covering >80% of the entire tissue were analyzed using the same profile file with the following characteristics: noise reduction (median filter strength = 3), object definition (HSV: 44 < Hue < 115, 36 < Saturation < 196, 5 < Value < 250; filtering by size: valid objects > 15 µm²) and object separation according to a 10-pixel distance between the center points of the two objects. These settings allowed the automatic segmentation of the detected objects and the measurement of the number of detected objects per mm².

Statistical analyses were performed on individual raw data using unpaired *t*-tests to compare the MAB-treated group to the PBS-treated group. Values are expressed as mean \pm s.e.m. $P < 0.05$ were considered statistically significant.

Collagen I detection by second-harmonic generation

FL lymph nodes or cells were embedded in tissue-freezing media and frozen at -80 °C. Then 5-µm sections were cut on a cryostat at -20 °C. The slides were mounted in Fluorescence Mounting Medium (DAKO). Collagen detection was performed using a two-photon microscope 7MP upright microscope (Zeiss). Excitation light was provided by a Chameleon Ultra II Ti:Sapphire laser (Chameleon Ultra, Coherent Inc., Palo Alto, CA, USA) tuned to 830 nm. The average laser irradiation after the microscope objective was measured with an Ultracompact Laser Power Meter (New Focus Corp., Irvine, CA, USA), which ranged from 0.5 to 2 mW. The second-harmonic generation images were detected through a bandpass filter SP 485 (collagen emission, Semrock, Rochester, NY, USA). Images were acquired using a $\times 40$ oil immersion objective (NA = 1.4, Plan-Apochromat; Zeiss). All images were acquired with standardized conditions for gain and offset (brightness and contrast). Unprocessed images were analyzed using the Region Measurements function of the Metamorph software (Universal Imaging, Downingtown, PA, USA), which calculates the integrated fluorescence intensity for the entire image.

For FL patient studies, institutional ethical approval from Inserm U1037 and informed consent were obtained in compliance with the Helsinki protocol.

Western blot analysis

MALC were dissociated with mechanical force in PBS. Cells were then washed with cold PBS and lysed in cytobuster protein extraction reagent (Novagen, Merck, Nottingham, UK) containing a protease inhibitor cocktail (Sigma-Aldrich). Western blot analyses were performed as previously described²⁴ using antibodies against laminin, fibronectin, vitronectin

(Sigma-Aldrich), cleaved caspase 3 (Ozyme, St Quentin en Yvelines, France), cleaved PARP (poly ADP-ribose polymerase; BD Pharmingen, Le Pont de Claix, France) and β -actin (Millipore, Molsheim, France). Peroxidase-conjugated secondary antibodies were from Jackson ImmunoResearch Laboratories (Immunotech, Marseille, France).

Apoptosis detection

MALC were dissociated as described above, and 10^5 cells were washed with cold PBS and resuspended in Binding Buffer 1X (BD Biosciences, Le Pont de Claix, France) at 1 m/ml. In all, 5 μ l Annexin V-PE (phycoerythrin) and 5 μ l 7AAD (7-aminoactinomycin D; BD Biosciences) were added for 15 min at room temperature in the dark, and then apoptotic cells (Annexin V⁺/7AAD⁻) were detected on a LSR II flow cytometer (BD Biosciences).

Lysosomal permeability detection

A total of 10^5 cells from dissociated MALC were incubated with 5 μ M acridine orange (Molecular Probes, Invitrogen, Life Technologies) for 15 min at room temperature in the dark. Cells were then washed twice with PBS and analyzed with LSR II flow cytometer.

Senescence-associated beta-galactosidase (SA- β gal) activity detection

To measure SA- β gal activity, we used the fluorogenic substrate C₁₂FDG (Invitrogen).²⁵ In all, 4×10^5 cells from dissociated MALC were pretreated with 100 nM bafilomycin A for 1 h at 37 °C 5% CO₂ to induce lysosomal alkalization and increase the internal pH of lysosomes to pH 6. C₁₂FDG (33 μ M) was then incubated for 2 h, after which the medium was removed. MALC were dissociated, cells were washed twice with PBS and analyzed with a LSR II flow cytometer.

Intracellular phosphospecific flow cytometry

Intracellular phosphospecific flow cytometry was performed as previously described.^{26,27} A total of 10^6 cells from dissociated MALC were fixed with BD Cytofix fixation buffer (BD Biosciences) for 10 min at room temperature. Cells were washed with wash buffer (BD Biosciences) and permeabilized with Perm Buffer III (BD Biosciences) for 30 min at 4 °C. Cells were washed, resuspended in cold 50% perm buffer III and mixed. Then either Cell Barcoding Dye 450 (BD Biosciences) at various concentrations (prepared according to the manufacturer's instructions) or dimethyl sulfoxide were added and incubated for 30 min at 4 °C. Cells were then washed and resuspended in a residual volume. Encoded samples were split equally into FACS (fluorescence-activated cell sorter) tubes for parallel stainings. Conjugated phosphospecific antibodies were added to each tube of cells for 30 min at room temperature. Antibodies against Akt-Alexa488, P-Akt(T308)-PE, P-Akt(S473)-Alexa647, Syk-FITC, P-ZAP70/Syk(Y319/Y352)-Alexa647, Phospholipase C, gamma 2 (PLC γ 2)-PE and P-PLC γ 2(Y759)-Alexa647 were all obtained from BD Biosciences. At least 50 000 events from each gated condition were collected and analyzed using a LSR II cytometer.

Mitochondrial depolarization assay

To evaluate the status of $\Delta\Psi$, we used a lipophilic fluorochrome JC-1 (5,5',6,6'-tetrachloro-1,1',3,3'-tetraethylbenzimidazolcarbocyanine iodide)

with the mitochondrial membrane potential detection kit (BD Biosciences) according to the manufacturer's instructions. To assess mitochondrial depolarization, untreated (UT) or treated MALC were dissociated and then stained with JC-1 for 15 min at 37 °C in a CO₂ incubator. Once washed and re-suspended in PBS, the loss of red fluorescence was monitored using flow cytometry.

Cytochrome c release assays

To evaluate cytochrome c release, we used anti-cytochrome c-Alexa 488 antibodies (BD Biosciences) according to the manufacturer's instructions. Treated or UT MALC were dissociated and then fixed and permeabilized with, respectively, BD Cytofix fixation buffer and BD Perm Buffer III before staining with an anti-cytochrome c antibody for 1 h at room temperature. Cytochrome c release was monitored by analyzing green fluorescence in the FL-1 channel with flow cytometry.

Mitochondrial ROS

Mitochondrial ROS were detected using a method previously published.²⁸ Briefly, 2×10^5 cells from UT or treated MALC were stained with Mitotracker deep red and Mitotracker green (Invitrogen) at 50 nM for 30 min at 37 °C. Cells were then washed with PBS and re-suspended in cold PBS for FACS analysis.

Sub-G1 cell determination after DAPI (4,6-diamidino-2-phenylindole) staining

Untreated or treated MALC were dissociated and transferred to 96-well-plates. Cells were then incubated in 70% EtOH for 30 min at 4 °C, washed twice and incubated with RNase A at 100 μ g/ml (Sigma-Aldrich) for 15 min at room temperature and then washed and incubated with DAPI (Sigma Aldrich) at 10 μ g/ml for 45 min at room temperature. Cells were analyzed using flow cytometry, and cell death was estimated by the percentage of sub-G1 cells.

Statistics

Data shown represent mean \pm s.d. Means were compared using unpaired, two-tailed Student's *t* tests, and *P* < 0.05 were considered statistically significant.

RESULTS

GA101 and RTX display comparable efficacy in a 2D RL culture model

RL are FL cells carrying the t(14; 18) translocation leading to Bcl-2 overexpression. In 2D RL cultures, we previously showed that RTX induces a moderate accumulation of cells in G1 phase, growth inhibition and significant loss in clonogenic potential.²⁹ Here, we determined the effect of GA101 compared with RTX and showed that both antibodies decrease RL cell viability to a similar degree (Figure 1a). By analyzing cell death using Annexin V/7AAD labeling, we observed only a slight increase in cells in early (Annexin V⁺/7AAD⁻) and late (Annexin V⁺/7AAD⁺) apoptosis

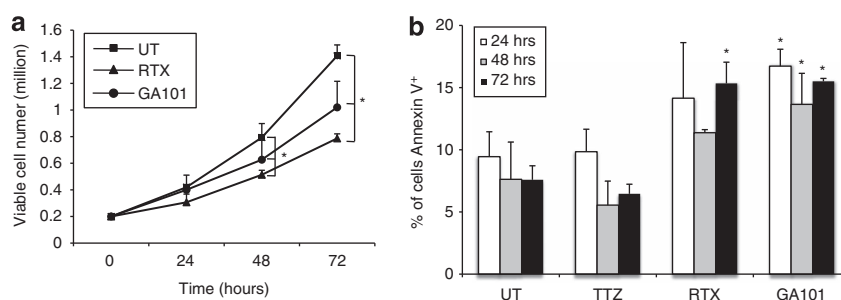


Figure 1. Effect of RTX and GA101 on 2D-cultured RL cells. **(a)** Cell viability of RL cells treated or not with 10 μ g/ml of RTX or GA101 was analyzed by exclusion of Trypan blue. **(b)** Percentage of cells in early and late apoptosis (Annexin V⁺/7AAD⁻ and Annexin V⁺/7AAD⁺) were determined by flow cytometry after 24, 48 and 72 h of treatment. Results are mean \pm s.d. of at least three independent experiments. **P* < 0.05 compared with UT cells.

after RTX and GA101 treatment. No significant differences were observed between the two antibodies (Figure 1b).

GA101 displays enhanced MALC growth inhibition

In order to investigate the role of spatial organization, we created the 3D MALC model using RL cells.²² MALC grew as oblate and relatively stiff spheroids (Figure 2A). MALC volume increased linearly with time (Figure 2B), whereas the number of cells increased exponentially throughout the culture (Figure 2C). No necrosis was observed during MALC culture (Figure 2D).

MALC stiffness could be due to an accumulation of extracellular matrix, as immunohistochemistry and western blotting showed the presence of fibronectin, vitronectin and laminin, similar to that

observed in RL xenografts or patient biopsies (Figures 2Ea and Eb). Collagen I was also found in MALC and FL tissues (Figure 2Ec).

We then sought to determine the effects of RTX and GA101 in 3D RL culture. To obtain the optimal dose of each antibody, we compared doses ranging from 0.1 to 100 $\mu\text{g}/\text{ml}$. Both antibodies showed a maximal effect on MALC volume, viable cell number and cell death at 10 $\mu\text{g}/\text{ml}$. The same results were obtained with MALC made up of diffuse large B-cell lymphoma (DEAU, Supplementary Figure S1A) and Burkitt lymphoma (Raji) (data not shown) cell lines. However, after 10 days of 3D culture >50% of Raji and DEAU cells were apoptotic under UT conditions, therefore we focused this study on MALC obtained with RL cells.

We first sought to assess TV over time following treatment with RTX, GA101 or Trastuzumab (used as negative control; data not shown). In UT cells, MALC volume increased from day 1 to day 20,

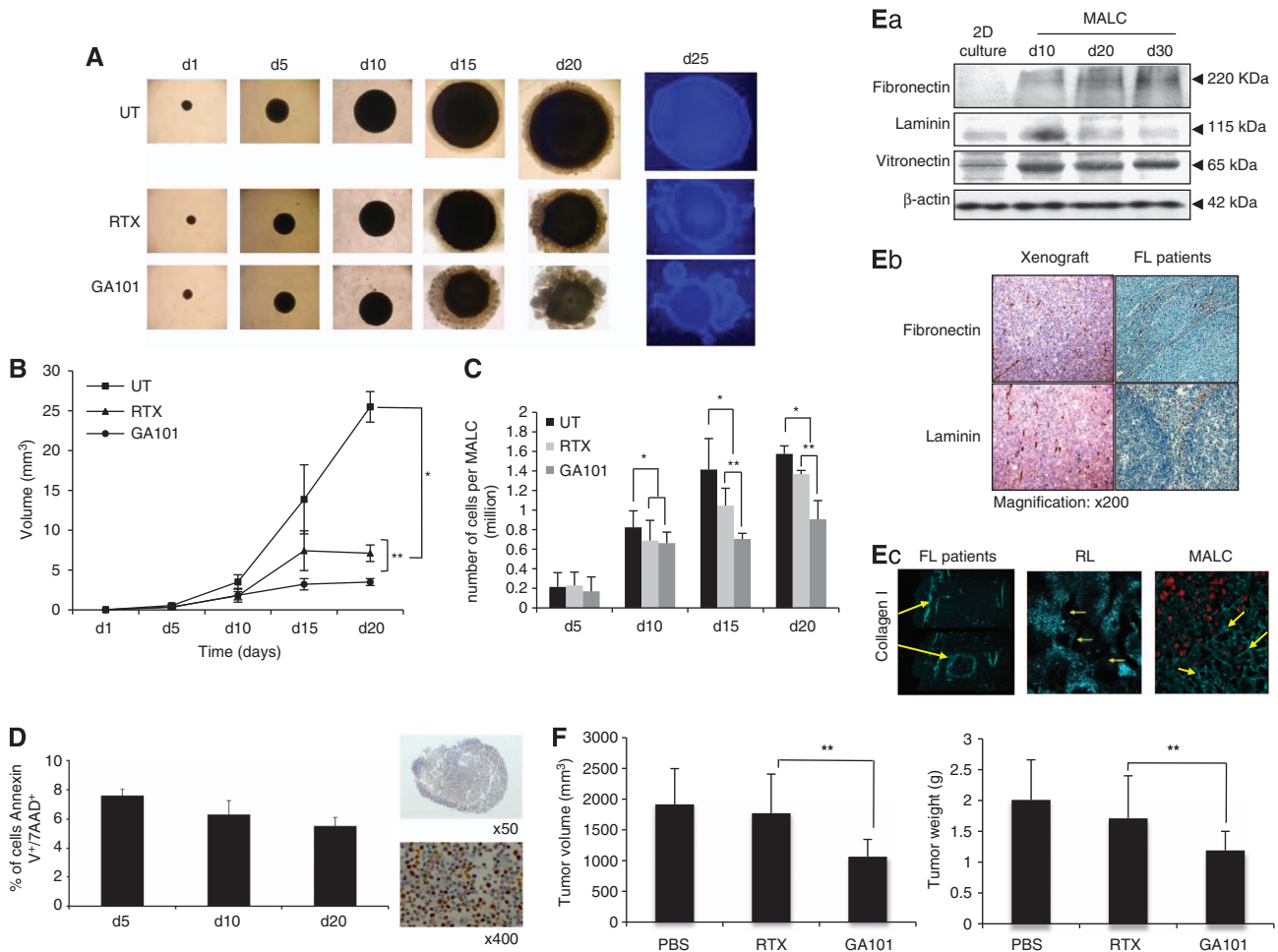


Figure 2. Effect of RTX and GA101 on MALC. **(A)** Pictures of treated or UT MALC were taken with an inverted Nikon Eclipse TE200 microscope at magnification $\times 40$ at different times of culture with or without Hoechst 33342 staining. These pictures are representative of several experiments ($d = \text{day}$). **(B)** MALC were treated or not (■) with 10 $\mu\text{g}/\text{ml}$ RTX (▲) or GA101 (●). MALC volume was measured at different times of culture. Results are expressed in mm^3 and represent the mean \pm s.d. of nine independent experiments. Asterisk represents significant differences between UT and anti-CD20 MAb treatment ($P < 0.05$); double asterisks represents significant differences between RTX and GA101 treatment ($P < 0.05$); ($d = \text{day}$). **(C)** Number of viable cells per treated or UT MALC over time. Histograms represent mean \pm s.d. of nine independent experiments. Asterisk represents significant differences between UT and anti-CD20 MAb treatment ($P < 0.05$); double asterisks represents significant differences between RTX and GA101 treatment ($P < 0.05$); ($d = \text{day}$). **(D)** Left panel: necrosis was determined by flow cytometry analyzing Annexin V⁺/7AAD⁺ cells in MALC at 5, 10 and 20 days. Right panel: Ki67 immunohistochemistry labelling in MALC at day 10. **(Ea)** Fibronectin, laminin and vitronectin expression analyzed by western blotting in MALC compared with 2D RL cells. β -Actin expression was used as a control of protein expression. **(Eb)** Fibronectin and laminin labelling on paraffin sections of RL xenografts or lymph nodes isolated from FL patients. **(Ec)** Collagen I (yellow arrows) was visualized by second-harmonic generation in a lymph node from FL patients (left) and MALC (right). Results are representative of three independent experiments. **(F)** TV and tumor weight were measured after RL engraftment onto SCID-Beige mice. Histograms represent the mean \pm s.d. of 9 animals for PBS, 9 animals for RTX and 10 animals for the GA101-treated group. Double asterisks represents significant differences between RTX and GA101 treatment ($P < 0.05$).

maintaining the spherical structure (Figure 2A) and reaching 25 mm³ (Figure 2B), with 1.5 million viable cells/MALC (Figure 2C). RTX and GA101 treatment induced potent morphological changes with a disintegration of the peripheral layer (Figure 2A), significantly reduced MALC growth (Figure 2B) and significantly decreased the number of viable cells/MALC (Figure 2C) without modifying cell size (determined by flow cytometry, data not shown). These effects appeared significantly more pronounced in MALC treated with GA101 compared with RTX.

We further evaluated the *in vivo* effects of the two antibodies in a RL xenograft mouse model. As shown in Figure 2F, GA101 inhibited tumor growth more strongly in terms of TV and tumor

weight compared with RTX-treated animals. No such differences in antibody activity were seen in 2D RL cultured with GA101 when compared with RTX, supporting the conclusion that the spatial organization existing in 3D culture and *in vivo* affects the sensitivity to antibody treatment.

GA101 induces cell death more robustly than RTX in MALC

The decrease in viable cell number in RTX or GA101-treated MALC observed in Figure 2C might reflect either a cell-cycle blockade or induction of cell death. Thus, we analyzed cell-cycle distribution and cyclin A, B and D₁ expression as key regulators of the S, G₂/M

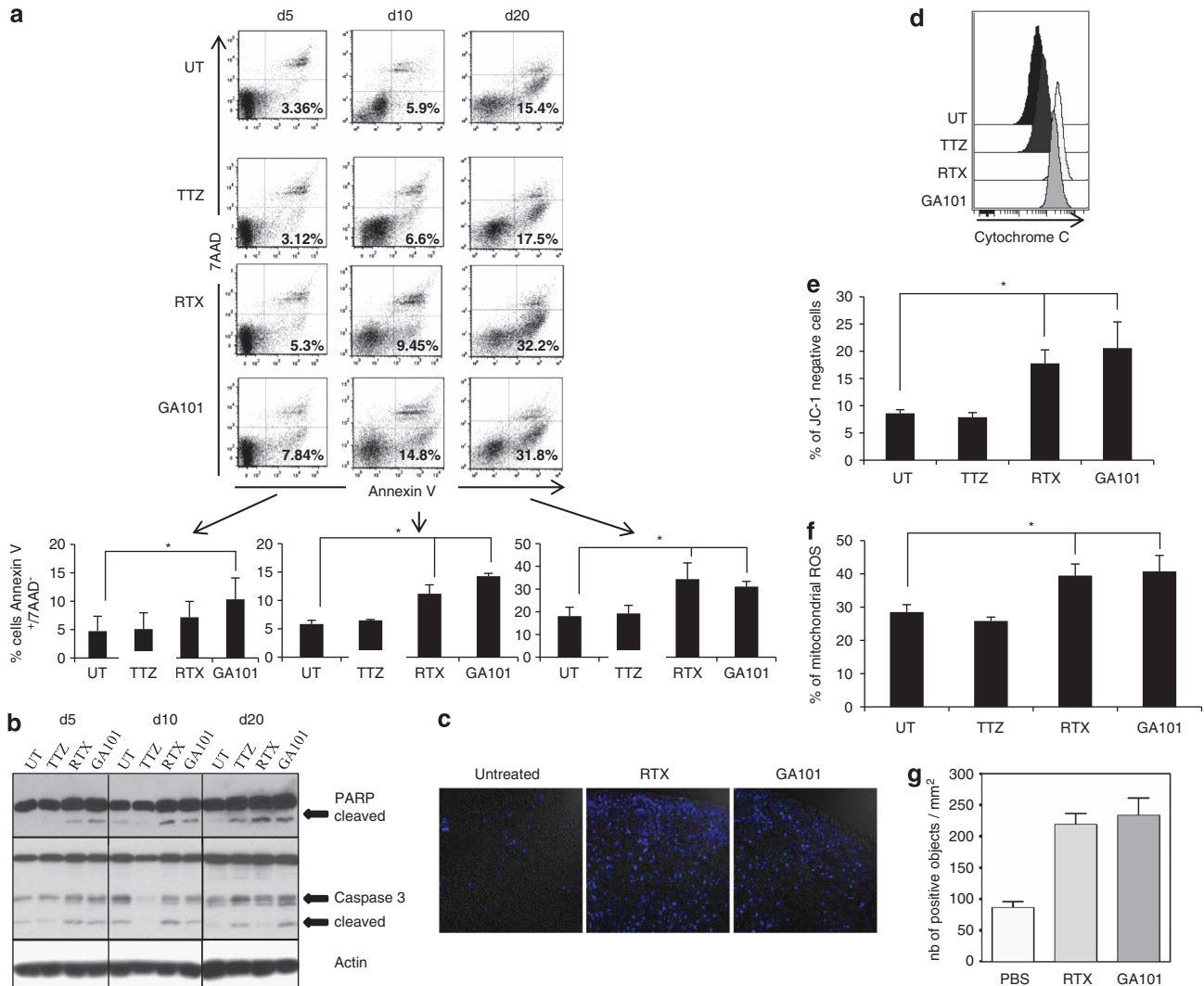


Figure 3. Induction of MALC apoptosis by RTX and GA101. (a) MALC were treated or not with 10 µg/ml of Trastuzumab (TTZ), RTX or GA101 for 5–20 days (d). Early apoptotic cells (Annexin V⁺/7AAD⁻) were detected by flow cytometry. Dot plots are representative of one experiment, and histograms represent the mean ± s.d. of FIVE independent experiments. Asterisk represents significant differences between UT and anti-CD20 MAb treatment ($P < 0.05$). (b) Detection of PARP and caspase 3 by western blot analysis in MALC treated or not with 10 µg/ml of TTZ, RTX or GA101 for 5–20 days (d). Results are representative of three independent experiments. β-Actin expression was used as a control of protein expression. (c) Caspase 3 detection by confocal microscopy in fixed and embedded representative MALC treated or not with 10 µg/ml of RTX or GA101 for 20 days. Magnification × 40. (d) Detection of cytochrome c release from mitochondria using flow cytometry in MALC treated or not with 10 µg/ml of TTZ, RTX or GA101 for 20 days. Histograms were analyzed with Cytobank (www.cytobank.org) and are representative of three independent experiments. (e) Mitochondrial depolarization was analyzed by flow cytometry in MALC treated (10 µg/ml antibody) or not for 20 days. Histograms represent the mean percentage of red-JC-1-negative cells for four independent experiments ± s.d. Asterisk represents significant differences between UT and anti-CD20 MAb treatment ($P < 0.05$). (f) ROS production was measured in MALC treated or not for 20 days with 10 µg/ml TTZ, RTX or GA101 by flow cytometry. Cells producing ROS were analyzed by double staining with Mitotracker green⁺/Mitotracker deep red⁻, and results represent the mean percentage of four independent experiments ± s.d. Asterisk represents significant differences between UT and anti-CD20 MAb treatment ($P < 0.05$). (g) Active caspase 3 quantification was performed on tumors derived from FL xenograft SCID-Beige mice injected intraperitoneally with PBS or with antibodies at 25 mg/kg twice a week.

and G0/G1 phase check points, respectively. Both cell-cycle distribution and expression of cyclins were not affected by RTX or GA101 treatment. Moreover, the proliferation rate did not differ between UT and MAb-treated conditions (data not shown). We therefore examined whether RTX and GA101 would induce apoptotic cell death, non-apoptotic (lysosomal) cell death or senescence, as reported elsewhere.^{2,3,12,13,30} We observed that both RTX and GA101 increased apoptotic cell death, with GA101 eliciting its effects earlier than RTX (Figure 3a). Anti-CD20 MAb-induced apoptosis was also observed in MALC realized with Deau cells (Supplementary Figure S1B). To avoid possible misinterpretation due to flow cytometry as previously described,³¹ the induction of apoptotic cell death by both RTX and GA101 was confirmed by western blot analysis revealing cleavage of caspase 3 and PARP (Figure 3b). In order to confirm the results obtained on disaggregated MALC, we performed caspase 3 active staining on fixed and embedded MALC. As shown in Figure 3c, RTX and GA101 induced an increase of apoptosis compared with UT MALC. In addition, RTX and GA101 caused cytochrome *c* release from mitochondria (Figure 3d), loss of $\Delta\Psi_m$ (Figure 3e) and production of ROS (Figure 3f). Apoptotic cell death induction was also confirmed *in vivo* from tumors isolated from GA101- and RTX-treated animals (Figure 3g).

In 2D RL cells treated as MAb-treated 3D cultures (that is, every 5 days), we observed a very slight induction of apoptosis in MAb-treated cells without any difference between RTX and GA101 (Supplementary Figure S2).

Interestingly, *in vitro* only GA101-treated MALC exhibited an increase in lysosomal cell death and cathepsin D release (Figure 4a and Supplementary Figure S1C for Deau cells). Furthermore, a senescence phenotype was found in GA101-treated cells, as shown by an increase in C_{12} FDG cleavage (Figure 4b). A similar effect was also observed following treatment with Cisplatin and Etoposide, both classical inducers of senescence (Figure 4b).

Altogether, these results demonstrate that both MAbs induce the same extent of apoptosis but GA101—but not RTX—induces lysosomal cell death and senescence.

GA101 induces a stronger signaling inhibition than RTX in MALC. We have previously shown that RTX reduced FL survival in 2D RL culture through inhibition of the PKC ξ -mTOR (mammalian target of rapamycin) module without affecting PI3K/Akt.³² Here, we observed that, unlike RTX, GA101 does decrease Akt phosphorylation, as evaluated by fluorescent cell barcoding

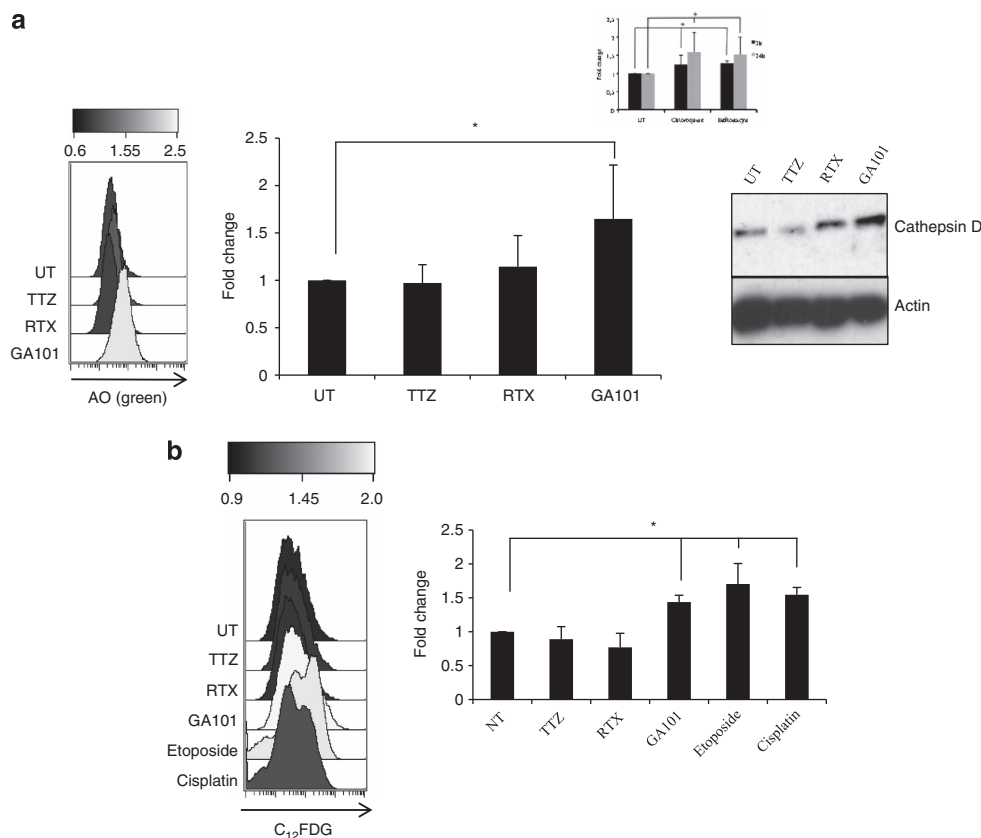


Figure 4. GA101 induces lysosomal cell death (a) and senescence (b) in MALC. (a) Left panel: Detection of lysosomal membrane permeabilization after acridine orange (AO) staining of MALC treated or not with 10 μ g/ml antibodies for 20 days. Box shows overlay of fold changes compared with UT MALC for one representative experiment. Histograms represent the mean fold change \pm s.d. of five independent experiments. * $P < 0.05$. Analysis and representation were performed with Cytobank. Insert: 2D RL culture cells treated with 50 μ M chloroquine or 50 nM bafilomycin for 3 or 24 h were used as positive controls for lysosomal cell death. Right panel: MALC were treated (10 μ g/ml antibodies) or not for 20 days, and cathepsin D expression was determined by western blot analysis. Results are representative of three independent experiments. β -Actin expression was used as a control of protein expression. (b) Detection of cleavage of C_{12} FDG by SA- β Gal was measured by an increase in green fluorescence in treated and UT MALC after 20 days of culture. 2D RL culture cells treated with 2.2 μ M cisplatin or 0.9 μ M etoposide for 3 days were used as a positive control of senescence. Left: Overlays of fold changes comparing treated to UT cells in one representative experiment. Right: Histograms represent the mean fold change \pm s.d. of five independent experiments * $P < 0.05$. Analysis and representation were performed with Cytobank.

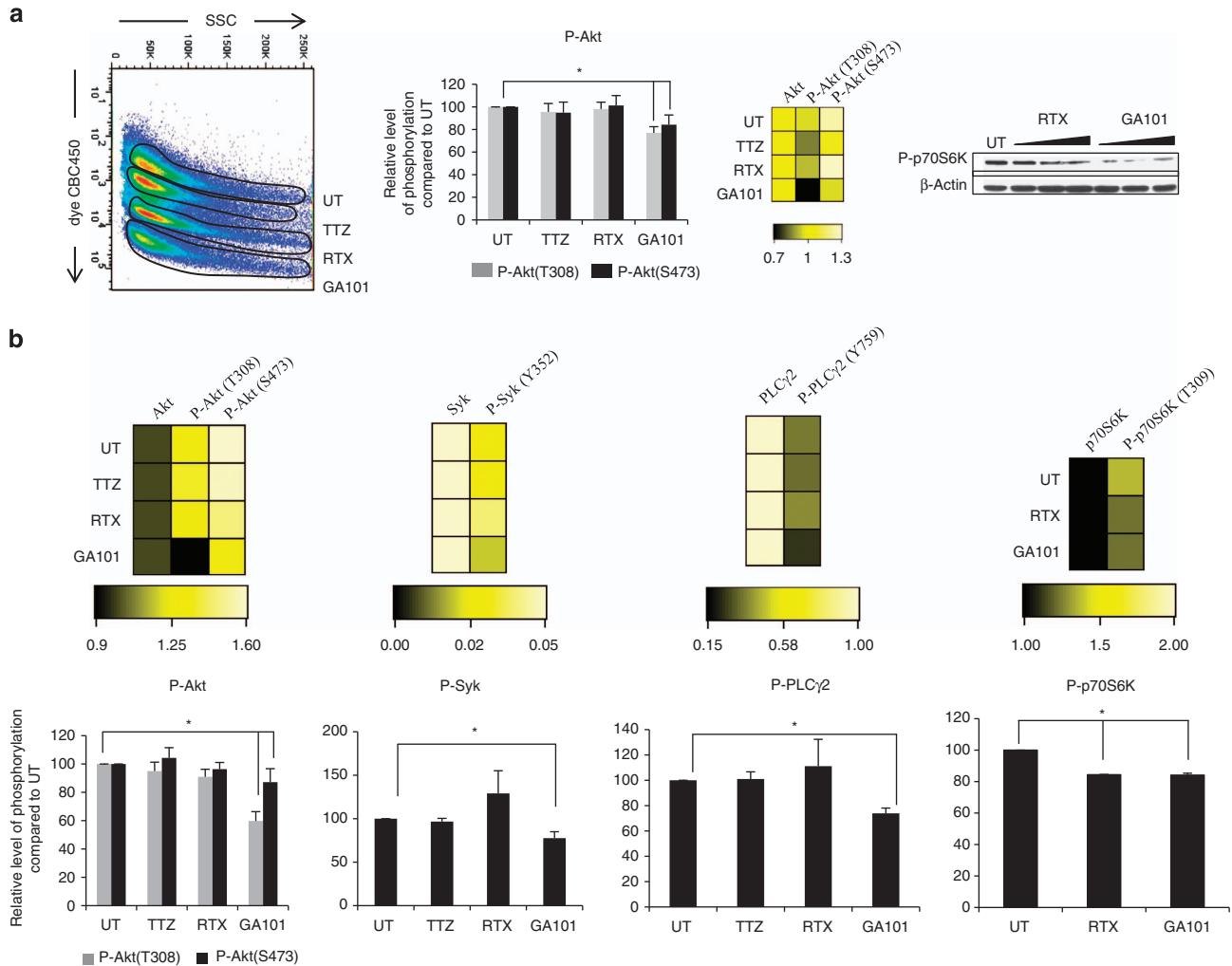


Figure 5. GA101 affects MALC signaling pathways. Cell signaling was analyzed as described in Materials and Methods. Dot plots represent all encoded conditions discriminated according to the CBD450 fluorescence of either 2D RL cells treated for 72 h with 10 μg/ml antibody (a) or MALC after 20 days of antibody treatment (b). Phosphospecific stainings were analyzed for each gated condition and heatmaps represent relative levels of phospho-Akt/Akt, phospho-Syk/Syk and phospho-PLCγ2/PLCγ2 for one representative experiment in RL treated or not for 72 h or in MALC treated or not at day 20. Analysis and representation were performed with Cytobank. Histograms represent the relative percentage of phosphorylated proteins in treated 2D (a) or 3D (b) cells compared with UT cells. Results represent mean ± s.d. of three independent experiments * $P < 0.05$. Western blot analysis of p70S6K phosphorylation was performed in 2D RL cells treated or not with 10 μg/ml antibody for 72 h (a).

(Figure 5a, left panel) and mTOR activation (Figure 5a, right panel). In 3D culture, GA101 inhibited phosphorylation of Akt at both T308 and S473, Syk at Y352 and PLCγ2 at Y759 as well as mTOR-dependant p70S6K phosphorylation at T389 (Figure 5b). RTX reduced mTOR phosphorylation (Figure 5c) but had no effect on the other kinases (Figure 5b).

Together, these results demonstrate that GA101 directly inhibits cell signaling in 3D FL culture and does so more efficiently than RTX.

Both GA101 and RTX antibodies induce chemosensitization

Previous studies have shown that when combined with chemotherapy both RTX and GA101 enhance efficacy or sensitize cells to cytotoxic drugs.^{33,34} Thus, we asked whether in 3D models antibodies could improve sensitivity to anti-tumoral drugs such as doxorubicin (anthracyclin), bendamustine (an alkylating agent) and rapamycin (an mTOR inhibitor). We

treated MALC via two distinct protocols. Protocol 1 (Figure 6a) involved adding the antibody to the drop at the beginning of MALC formation followed by treatment with the cytotoxic drugs 24 h later. In protocol 2 (Figure 6b), established MALC were treated with antibodies (after 5 days of 3D culture) followed by addition of cytotoxic drugs 24 h later. In both protocols, we did not observe sensitization to doxorubicin or to bendamustine (data not shown). However, both antibodies sensitized the 3D-cultured cells to treatment with rapamycin (Figure 6). These results show that both RTX and GA101 sensitize 3D FL cultures to rapamycin.

DISCUSSION

To develop new therapeutic strategies (that is, new anti-CD20 antibodies), we need a better understanding of the *in vitro* mechanisms of action of these therapies. For classical 2D NHL cell cultures, we and others have described the mechanisms that

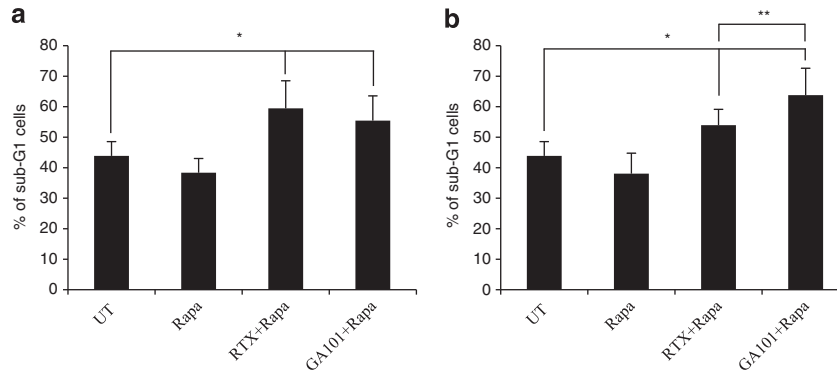


Figure 6. Antibodies sensitize MALC to rapamycin. MALC were treated in the drop (**a**) or after 5 days of culture (**b**) with 10 $\mu\text{g/ml}$ antibodies. Twenty-four hours later, MALC were treated with 50 nM of rapamycin. Every 5 days, cells were submitted to the same treatment. Results represent the percentage of cells in sub-G1 phase as determined by flow cytometry after DAPI staining at day 20 and are the mean of six independent experiments \pm s.d. Asterisk represents significant differences between UT and anti-CD20 MAb/rapamycin treatment ($P < 0.05$); Double asterisks represents significant differences between RTX/Rapa and GA101/Rapa treatment ($P < 0.05$).

account for the direct effect of the CD20 antibodies RTX and GA101.^{2,3,12,13} RTX and GA101 display similar efficiencies in the follicular NHL cell line RL; however, GA101 has been reported to mediate superior effects on 2D lymphoma cell lines, such as large B-cell lymphomas, mantle cell lymphoma and chronic lymphocytic leukemia.^{9,35}

The importance of tumor spatial organization is becoming increasingly apparent and can significantly affect major cellular functions such as cell proliferation, survival and intracellular signaling pathways, as described for carcinoma cell spheroids. Based on these models, we used NHL cell lines to create MALC with a technique derived from the hanging drop method. MALC mimic lymphoma spatial organization, including extracellular matrix accumulation. This model is simple, feasible, reproducible, inexpensive and offers an alternative to xenografts for testing new drugs. We observed that both RTX and GA101 displayed higher efficacy in MALC compared with 2D culture. This result was unexpected, as one could have hypothesized that the increased cellular density, higher degree of compaction and ECM accumulation would have interfered with the diffusion of the antibodies into the spheroid and their subsequent effects. It is possible that 3D FL cells are in a more sensitive state because of changes to intracellular signaling pathways as a result of mechanical stress, hypoxia or modified integrin signaling networks. Clinical observations have underlined tumor burden as potentially one of the most important factors mediating resistance to RTX.^{36,37}

This was recently confirmed in a study showing that mice presenting with a low tumor burden had a significantly higher complete response rate and a significant longer survival than mice with intermediate or high tumor burden.³⁸ One of the reasons for this may be differences in antibody diffusion and penetration into the center of small lymph nodes versus a less efficient diffusion in cases of high tumor burden. Our model provides a powerful approach to study this phenomenon.

Here, we show that, unlike in 2D culture, RTX and GA101 induce apoptotic cell death in FL cells when organized in 3D. To avoid possible misinterpretation due to flow cytometry as previously described,³¹ we confirmed cell death induction by western blot analysis of PARP and caspase 3 cleavage (on disaggregated or entire MALC), determination of cytochrome *c* release, $\Delta\Psi\text{m}$ modification and ROS production.

Recent reports have demonstrated that, in 2D-cultured NHL cell lines, GA101 induces homotypic adhesion followed by actin reorganization, lysosomal permeabilization, cathepsin release and ROS production. Altogether, these events suggest a so-called

non-apoptotic lysosomal-mediated cell death.^{12,13} In our 3D model, we detected lysosomal cell death and cathepsin D release after 20 days of GA101 treatment. This was also accompanied by senescence, a phenomenon described by Däbritz *et al.*³⁰ for RTX. Although this has never been described for GA101, it should not be surprising as senescence is an aging process involving ROS.³⁹ Autophagy has also been described after RTX treatment in Burkitt lymphoma cell lines.⁴⁰ However, we found no significant change in the expression of the autophagic proteins LC3II and Atg proteins following RTX or GA101 treatment using both protein micro-arrays and western blot analysis (data not shown). In terms of RTX treatment, we showed that 3D conditions enhanced RTX-induced cytotoxic effects, reflecting clinical observations. For GA101, we also observed an enhancement of cytotoxic effects in 3D- compared with 2D-cultured FL cells, perhaps a result of the combination of the three different cell death mechanisms (apoptosis, lysosomal cell death and senescence). The fact that GA101 displayed a higher efficacy than RTX is in accordance with observations from *in vitro* and preclinical studies^{9,12,33} (Figure 2F) and may be related to its type-II-related mechanism of action resulting in, for example, homotypic adhesion and cell death.⁴¹ GA101 could also affect cell-cell contacts supporting the 3D structure. Indeed, we used Hoechst labeling (Figure 2A) to observe that GA101 strongly modifies the spherical organization of NHL cultured in 3D. Moreover, we cannot exclude the possibility that GA101 and RTX diffuse differently into MALC. The mechanisms of diffusion are not yet known and are currently under investigation in our laboratory.

Previous studies show that RTX and GA101 induce chemosensitization in 2D NHL cultures and xenograft FL models.^{33,34} Consistent with this, we showed that both anti-CD20 antibodies induce sensitization to rapamycin (a classical mTOR inhibitor) in 3D culture. Chemosensitization can be explained by several hypotheses. First, it may be a consequence of decreased Bcl2 expression after 10 days of antibody treatment (Supplementary Figure S3), as Bcl2 expression has been associated with resistance to mTOR inhibitors in a preclinical model.⁴² Second, antibodies could affect the 3D structure (cell-cell contacts), leading to better drug penetration. This is currently under investigation in our laboratory. Third, chemotherapeutic agents and antibodies may use the same signaling pathways (that is, ROS production, inhibition of mTOR, and so on), converging on enhanced cytotoxic effects compared with those induced by each drug as a single agent.

Altogether, this study presents strong evidence that GA101 displays enhanced efficacy compared with RTX in a 3D NHL model that mimics lymphoma cell growth in an aggregated architecture. These findings support preclinical and *in vivo* studies and provide a useful model for further investigation of the molecular mechanisms involved in the anti-lymphoma action of antibodies.

CONFLICT OF INTEREST

ED, NV and AS are employees of Institut de Recherche Roche (Boulogne Billancourt, France), F. Hoffmann-La Roche AG (Basel, Switzerland) and Roche S.A.S. (Boulogne Billancourt, France) respectively. CB is an employee of Roche Glycart AG (Schlieren). SF received a grant from Roche. CK received research funding from Roche. The other authors declare no conflict of interest.

ACKNOWLEDGEMENTS

This study was supported by an institutional grant from the INSERM, Cancéropôle Grand Sud-Ouest, INCA Pair Lymphome and Roche. We thank Raphael Duran, Marie-Noelle Paludetto (CRCT, INSERM UMR1037) for performing preliminary experiments, Amandine Blanc (CRCT, INSERM UMR1037) for technical assistance Sophie Allart and Astrid Canivet (Imaging core Facility, CPTP, INSERM U1043, Toulouse, France) and Maryline Calyse (ANEXPLO/CREFRE, Service de Zootechnie, Toulouse, France). We thank Scientific Scripts (<http://www.scientificscripts.com/>) for English proofreading.

Trastuzumab (TTZ, Herceptin), Rituximab (RTX, Mabthera) and Obinutuzumab (GA101) were provided by Genentech (San Francisco, USA), Roche (Boulogne Billancourt, France) and Roche Glycart (Schlieren, Switzerland), respectively.

We also thank ImagIN Platform of the Institut Universitaire du Cancer (<https://www.imagin.univ-tlse3.fr/Imagin/index.php?lang=EN>).

AUTHOR CONTRIBUTIONS

ED designed and performed experiments, analyzed data and drafted the manuscript. CJ developed the MALC technology and performed *in vitro* experiments. FC and AM performed immunohistochemical staining. CL and TAS interpreted results. SF performed murine model and 2D RL cell culture experiments. FXF realized *in vivo* caspase 3 quantifications. GL, CK, JFF, NV and AS helped plan experiments and interpret data. CB designed the research plan, supervised experiments, interpreted results and wrote the manuscript.

REFERENCES

- 1 Maloney DG. Treatment of follicular non-Hodgkin's lymphoma. *Curr Hematol Rep* 2005; **4**: 39–45.
- 2 Bonavida B. Rituximab-induced inhibition of antiapoptotic cell survival pathways: implications in chemo/immunosensitivity, rituximab unresponsiveness, prognostic and novel therapeutic interventions. *Oncogene* 2007; **26**: 3629–3636.
- 3 Bezombes C, Fournié JJ, Laurent G. Direct effect of rituximab in B-cell-derived lymphoid neoplasias: mechanism, regulation, and perspectives. *Mol Cancer Res* 2011; **9**: 1435–1442.
- 4 Witzig TE, Gupta M. Signal transduction inhibitor therapy for lymphoma. *Hematology (Am Soc Hematol Educ Program)* 2010; **2010**: 265–270.
- 5 Mahadevan D, Fisher RL. Novel therapeutics for aggressive non-Hodgkin's lymphoma. *J Clin Oncol* 2011; **29**: 1876–1884.
- 6 Sawas A, Diefenbach C, O'Connor OA. New therapeutic targets and drugs in non-Hodgkin's lymphoma. *Curr Opin Hematol* 2011; **18**: 280–287.
- 7 Smith MR. Rituximab (monoclonal anti-CD20 antibody): mechanisms of action and resistance. *Oncogene* 2003; **22**: 7359–7368.
- 8 Taylor RP, Lindorfer MA. Immunotherapeutic mechanisms of anti-CD20 monoclonal antibodies. *Curr Opin Immunol* 2008; **20**: 444–449.
- 9 Mössner E, Brünker P, Moser S, Püntener U, Schmidt C, Herter S *et al*. Increasing the efficacy of CD20 antibody therapy through the engineering of a new type II anti-CD20 antibody with enhanced direct and immune effector cell-mediated B-cell cytotoxicity. *Blood* 2010; **115**: 4393–4402.
- 10 Ivanov A, Beers SA, Walshe CA, Honeychurch J, Alduaij W, Cox KL *et al*. Monoclonal antibodies directed to CD20 and HLA-DR can elicit homotypic adhesion followed by lysosome-mediated cell death in human lymphoma and leukemia cells. *J Clin Invest* 2009; **119**: 2143–2159.

- 11 Beers SA, Chan CH, James S, French RR, Attfield KE, Brennan CM *et al*. Type II (tositumomab) anti-CD20 monoclonal antibody out performs type I (rituximab-like) reagents in B-cell depletion regardless of complement activation. *Blood* 2008; **112**: 4170–4177.
- 12 Alduaij W, Ivanov A, Honeychurch J, Cheadle EJ, Potluri S, Lim SH *et al*. Novel type II anti-CD20 monoclonal antibody (GA101) evokes homotypic adhesion and actin-dependent, lysosome-mediated cell death in B-cell malignancies. *Blood* 2011; **117**: 4519–4529.
- 13 Honeychurch J, Alduaij W, Azizyan M, Cheadle EJ, Pelicano H, Ivanov A *et al*. Antibody-induced nonapoptotic cell death in human lymphoma and leukemia cells is mediated through a novel reactive oxygen species-dependent pathway. *Blood* 2012; **119**: 3523–3533.
- 14 Sehn LH, Assouline SE, Stewart DA, Mangel J, Gascoyne RD, Fine G *et al*. A phase 1 study of obinutuzumab induction followed by 2 years of maintenance in patients with relapsed CD20-positive B-cell malignancies. *Blood* 2012; **119**: 5118–5125.
- 15 Salles G, Morschhauser F, Lamy T, Milpied N, Thieblemont C, Tilly H *et al*. Phase 1 study results of the type II glycoengineered humanized anti-CD20 monoclonal antibody obinutuzumab (GA101) in B-cell lymphoma patients. *Blood* 2012; **119**: 5126–5132.
- 16 Klement G, Huang P, Mayer B, Green SK, Man S, Bohlen P *et al*. Multicellular gastric cancer spheroids recapitulate growth pattern and differentiation phenotype of human gastric carcinomas. *Gastroenterology* 2001; **121**: 839–852.
- 17 Dangles-Marie V, Richon S, El-Behi M, Echchakir H, Dorothée G, Thiery J *et al*. A three-dimensional tumor cell defect in activating autologous CTLs is associated with inefficient antigen presentation correlated with heat shock protein-70 down-regulation. *Cancer Res* 2003; **63**: 3682–3687.
- 18 Ghosh S, Spagnoli GC, Martin I, Ploegert S, Demougin P, Heberer M *et al*. Three-dimensional culture of melanoma cells profoundly affects gene expression profile: a high density oligonucleotide array study. *J Cell Physiol* 2005; **204**: 522–531.
- 19 Zietarska M, Maugard CM, Filali-Mouhim A, Alam-Fahmy M, Tonin PN, Provencher DM *et al*. Molecular description of a 3D *in vitro* model for the study of epithelial ovarian cancer (EOC). *Mol Carcinog* 2007; **46**: 872–885.
- 20 Weigelt B, Lo AT, Park CC, Gray JW, Bissell MJ. HER2 signaling pathway activation and response of breast cancer cells to HER2-targeting agents is dependent strongly on the 3D microenvironment. *Breast Cancer Res Treat* 2010; **122**: 35–43.
- 21 Pickl M, Ries CH. Comparison of 3D and 2D tumor models reveals enhanced HER2 activation in 3D associated with an increased response to trastuzumab. *Oncogene* 2009; **28**: 461–468.
- 22 Gravelle P, Jean C, Valleron W, Laurent G, Fournié JJ. Innate predisposition to immune escape in follicular lymphoma cells. *Oncimmunology* 2012; **1**: 555–556.
- 23 Sutherland R, Buchegger F, Schreyer M, Vacca A, Mach JP. Penetration and binding of radiolabeled anti-carcinoembryonic antigen monoclonal antibodies and their antigen binding fragments in human colon multicellular tumor spheroids. *Cancer Res* 1987; **47**: 1627–1633.
- 24 Leseux L, Hamdi SM, Al Saati T, Capilla F, Recher C, Laurent G *et al*. Syk-dependent mTOR activation in follicular lymphoma cells. *Blood* 2006; **108**: 4156–4162.
- 25 Debacq-Chainiaux F, Erusalimsky JD, Campisi J, Toussaint O. Protocols to detect senescence-associated beta-galactosidase (SA-beta-gal) activity, a biomarker of senescent cells in culture and *in vivo*. *Nat Protoc* 2009; **4**: 1798–1806.
- 26 Irish JM, Czerwinski DK, Nolan GP, Levy R. Kinetics of B cell receptor signaling in human B cell subsets mapped by phosphospecific flow cytometry. *J Immunol* 2006; **177**: 1581–1589.
- 27 Irish JM, Myklebust JH, Alizadeh AA, Houot R, Sharman JP, Czerwinski DK *et al*. B-cell signaling networks reveal a negative prognostic human lymphoma cell subset that emerges during tumor progression. *Proc Natl Acad Sci USA* 2010; **107**: 12747–12754.
- 28 Zhou R, Yazdi AS, Menu P, Tschopp J. A role for mitochondria in NLRP3 inflammasome activation. *Nature* 2011; **469**: 221–225. Erratum in: *Nature* 2011; **475**: 122.
- 29 Bezombes C, Grazide S, Garret C, Fabre C, Quillet-Mary A, Müller S *et al*. Rituximab antiproliferative effect in B-lymphoma cells is associated with acid-sphingomyelinase activation in raft microdomains. *Blood* 2004; **104**: 1166–1173.
- 30 Däbritz JHM, Yu Y, Rosenfeldt MT, Dörken B, Schmitt CA. Anti-CD20 immunotherapy augments the chemotherapy-induced senescence response in human lymphoma cells. *Blood (ASH Annual Meeting Abstracts)* 2010; **118**: (abstract 1827).
- 31 Golay J, Bologna L, André PA, Buchegger F, Mach JP, Boumsell L *et al*. Possible misinterpretation of the mode of action of therapeutic antibodies *in vitro*: homotypic adhesion and flow cytometry result in artefactual direct cell death. *Blood* 2010; **116**: 3372–3373.
- 32 Leseux L, Laurent G, Laurent C, Rigo M, Blanc A, Olive D *et al*. PKC zeta mTOR pathway: a new target for rituximab therapy in follicular lymphoma. *Blood* 2008; **111**: 285–291.
- 33 Dalle S, Reslan L, Besseyre de Horts T, Herveau S, Herting F, Plesa A *et al*. Preclinical studies on the mechanism of action and the anti-lymphoma activity of the novel anti-CD20 antibody GA101. *Mol Cancer Ther* 2011; **10**: 178–185.

- 34 Jazirehi AR, Bonavida B. Cellular and molecular signal transduction pathways modulated by rituximab (rituxan, anti-CD20 mAb) in non-Hodgkin's lymphoma: implications in chemosensitization and therapeutic intervention. *Oncogene* 2005; **24**: 2121–2143.
- 35 Patz M, Isaeva P, Forcob N, Müller B, Frenzel LP, Wendtner CM *et al*. Comparison of the in vitro effects of the anti-CD20 antibodies rituximab and GA101 on chronic lymphocytic leukaemia cells. *Br J Haematol* 2011; **152**: 295–306.
- 36 Berinstein NL, Grillo-López AJ, White CA, Bence-Bruckler I, Maloney D, Czuczman M *et al*. Association of serum Rituximab (IDEC-C2B8) concentration and anti-tumor response in the treatment of recurrent low-grade or follicular non-Hodgkin's lymphoma. *Ann Oncol* 1998; **9**: 995–1001.
- 37 Maloney DG. Follicular NHL: from antibodies and vaccines to graft-versus-lymphoma effects. *Hematology (Am Soc Hematol Educ Program)* 2007 226–232.
- 38 Daydé D, Ternant D, Ohresser M, Lerondel S, Pesnel S, Watier H *et al*. Tumor burden influences exposure and response to rituximab: pharmacokinetic-pharmacodynamic modeling using a syngeneic bioluminescent murine model expressing human CD20. *Blood* 2009; **113**: 3765–3772.
- 39 Hekimi S, Lapointe J, Wen Y. Taking a "good" look at free radicals in the aging process. *Trends Cell Biol* 2011; **21**: 569–576.
- 40 Turzanski J, Daniels I, Haynes AP. Involvement of macroautophagy in the caspase-independent killing of Burkitt lymphoma cell lines by rituximab. *Br J Haematol* 2009; **145**: 137–140.
- 41 Niederfellner G, Lammens A, Mundigl O, Georges GJ, Schaefer W, Schwaiger MO *et al*. Epitope characterization and crystal structure of GA101 provide insights into the molecular basis for type I/II distinction of CD20 antibodies. *Blood* 2011; **118**: 358–367.
- 42 Delbaldo C, Albert S, Dreyer C, Sablin MP, Serova M, Raymond E *et al*. Predictive biomarkers for the activity of mammalian target of rapamycin (mTOR) inhibitors. *Target Oncol* 2011; **6**: 119–124.



This work is licensed under a Creative Commons Attribution-NonCommercial-NoDerivs 3.0 Unported License. To view a copy of this license, visit <http://creativecommons.org/licenses/by-nc-nd/3.0/>

Supplementary Information accompanies this paper on Blood Cancer Journal website (<http://www.nature.com/bcj>)